The Lund-York-Cologne Calorimeter (LYCCA): Concept, Design and Prototype Developments for a FAIR-NUSTAR Detector System to Discriminate Relativistic Heavy-ion Reaction Products

Golubev, Pavel; Wendt, A.; Scruton, L.; Taprogge, J.; Rudolph, Dirk; Reiter, P.; Bentley, M. A.; Avdeichikov, Vladimir; Boutachkov, P.; Fox, S. P.; Gerl, J.; Goergen, Ch.; Hoischen, Robert; Kurz, N.; Singh, B. S. Nara; Pascovici, G.; Pietri, S.; Schaffner, H.; Taylor, M. J.; Thiel, S.; Wollersheim, H. J.

Published in:
Nuclear Instruments & Methods in Physics Research. Section A: Accelerators, Spectrometers, Detectors, and Associated Equipment

DOI:
10.1016/j.nima.2013.04.058

2013

The Lund-York-Cologne Calorimeter (LYCCA): Concept, design and prototype developments for a FAIR-NUSTAR detector system to discriminate relativistic heavy-ion reaction products

P. Golubev[a], A. Wendt[b], L. Scruton[c], J. Taprogge [1,2,b], D. Rudolph[a], P. Reiter[b], M.A. Bentley[c], V. Avdeichikov[a], P. Boutachkov[d,e], S.P. Fox[c], J. Gerl[d], Ch. Görgen[b], R. Hoischen [3,a,d], N. Kurz[d], B.S Nara Singh[c], G. Pascovici[b], S. Pietri[d], H. Schaffner[d], M.J. Taylor [4,c], S. Thiel[b], H.J. Wollersheim[d]

[a] *Department of Physics, Lund University, SE-22100 Lund, Sweden*
[b] *Institut für Kernphysik, Universität zu Köln, D-50937 Köln, Germany*
[c] *Department of Physics, University of York, York YO10 5DD, United Kingdom*
[d] *GSI Helmholtzzentrum für Schwerionenforschung GmbH, D-64291 Darmstadt, Germany*
[e] *Institut für Kernphysik, Technische Universität Darmstadt, D-64289 Darmstadt, Germany*

Abstract

The concept, design and prototype developments for the Lund-York-Cologne CAlorimeter (LYCCA) is presented. LYCCA is a modular device for the NUclear STructure, Astrophysics and Reactions (NUSTAR) science pillar of the Facility for Antiproton and Ion Research (FAIR) at Darmstadt, Germany. LYCCA is designed to discriminate heavy ions produced in nuclear reactions induced by relativistic radioactive ion beams. Measurements of energy loss, total energy, and time-of-flight allows the derivation of proton number, Z, and mass number, A, of the reaction products. LYCCA-inherent tracking of the flight paths of the reaction products enables coincident HIgh-resolution in-beam γ-ray SPECtroscopy (HISPEC) of atomic nuclei far from the line of β-stability.

Keywords: relativistic heavy ions, nuclear structure, time of flight, energy loss, total energy, A and Z identification

1. Introduction and Requirements

The NUclear STructure, Astrophysics and Reactions (NUSTAR) science pillar [1] of the Facility for Antiproton and Ion Research (FAIR) at Darmstadt, Germany awaits beams of relativistic radioactive ions with unprecedented intensities. The major incentive is to study the atomic nucleus at its extremes of proton-to-neutron ratio, which is of immediate relevance towards and motivated by heavy-element production in the course of stellar evolution.

The HIgh-resolution in-beam SPECtroscopy (HISPEC) [2] experiment within NUSTAR addresses nuclear structure questions by using radioactive beams to be delivered by the new, super-conducting FRagment Separator (Super-FRS) [3]. The beam energies are typically some 100-300 MeV/u. Single-step Coulomb excitation and nuclear fragmentation reactions at these intermediate energies as well as inelastic scattering, transfer and knock-out reactions are envisaged. The experiments will provide information relevant for the shell structure of atomic nuclei far from the line of β-stability, and more specifically low-lying excitation energies, transition probabilities, or single-particle spectroscopic factors, to name but a few.

The core of HISPEC is the use of high-resolution Ge detectors at one of the focal planes of the Super-FRS, i.e. to perform high-resolution in-beam spectroscopy of excited nuclear quantum states via their γ-ray decay; therefore, the HISPEC set-up foresees at its core the European Advanded GAmma-ray Tracking Array (AGATA) [4], surrounding the secondary target position. To enable event-by-event correlations of the γ rays with the nuclear residues, HISPEC will comprise a new generation of beam tracking and identification detectors placed in front of and behind the secondary target. Here, the Lund-York-Cologne CAlorimeter (LYCCA) has the central role of determining both proton number, Z, and mass number, A, of the final reaction products; by itself or in conjunction with a magnetic spectrometer. Until HISPEC becomes operational, a subset of LYCCA detectors is being commissioned and used for

Email address: Pavel.Golubev@nuclear.lu.se (P. Golubev)

the PRESPEC-AGATA [5] physics campaign at the existing FRS facility [6] at the GSI Helmholtzcentre for Heavy Ion Research in Darmstadt, Germany.

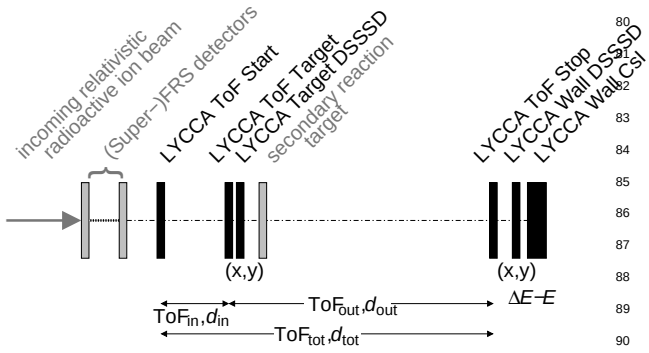

Figure 1: Sketch of the detection concept of LYCCA. LYCCA-related items are drawn in black. See text for details.

HISPEC-type experiments have also been performed already within the Rare Isotope Spectroscopic INvestigations at GSI (RISING) Fast-Beam campaign 2003–2005 [7]. Here, γ-ray spectroscopy with fifteen former EUROBALL Cluster detectors [8] was performed in conjunction with the CAlorimeter TElescope (CATE) [9], which at the time provided discrimination between nuclear reaction products. Both the experience with CATE and extensive simulations within the LYCCA collaboration [10] show that several items are essential for an improved HISPEC calorimeter system:

- A physical segmentation of both ΔE and E elements is useful for both rate considerations and active tracking.
- To achieve a proper mass separation, a high-precision time-of-flight system (better than 50 ps FWHM resolution [10]) needs to be integrated.
- LYCCA should be able to deal with rather light nuclei, $A \sim 30$, at energies up to 300 MeV/u, likewise heavy nuclei, $A \sim 200$, down to about 100 MeV/u.

The resulting LYCCA detection concept within the HISPEC framework is sketched in Fig. 1: Up front, the definition of the tracked position and proton number, Z, as well as mass number, A, of the incoming relativistic radioactive ion beam is subject to either future Super-FRS or existing FRS detection systems. A double-sided silicon strip detector (DSSSD) at the secondary target position together with those forming the downstream LYCCA wall ensure precise (x,y)-tracking of the reaction products. At the same time, the DSSSD wall elements provide an energy-loss signal, ΔE, which in conjunction with the measurement of the residual energy, $E_{\rm res}$, of the recoiling reaction products aims at determining their proton number, Z, by means of the established ΔE-$E_{\rm res}$ technique. E_{res} is determined by LYCCA wall CsI(Tl) detector elements. The DSSSD position measurement also has the capacity to improve CsI energy resolution through straightforward corrections of possible CsI light-collection dependencies on the impact position of the ions.

To determine the mass number, A, of the reaction products, E_{res} is being correlated with time-of-flight (ToF) information (cf. Ref. [10]), in particular by measuring $\mathrm{ToF_{out}}$ over the distance $d_{\rm out}$ between the LYCCA ToF Target and LYCCA ToF Stop detectors. The thickness of the secondary target used in previous in-beam campaigns seriously limited the envisaged mass resolution of the CATE spectrometer. This was especially worsened in fragmentation reactions due to the momentum spread induced by the reaction process. Therefore, available flight-paths and required solid-angle coverage call for a high-precision timing measurement. Simulations indicate [10] that a timing resolution of 50 ps (FWHM) or better is required, though this number depends on recoil energies and the mass regimes of interest. The ToF Target detector is placed near the secondary target inside the target chamber, the ToF Stop detector close to the LYCCA wall DSSSD elements. In addition, the individual velocities of incoming beam particles can be re-determined with $\mathrm{ToF_{in}}$ between the LYCCA ToF Start and LYCCA ToF Target detector over the distance $d_{\rm in}$.

Based on the LYCCA simulations [10] and anticipated typical HISPEC experiments and experimental conditions, the following design goals concerning A and Z resolution of LYCCA have been defined in the LYCCA Technical Design Report [11]:
DSSSD energy resolution (FWHM) at 0.1 GeV:
$\Delta E/E < 1$ %, projected goal $\Delta E/E < 0.5$ %
CsI(Tl) energy resolution (FWHM) at 10 GeV:
$\Delta E/E < 1$ %, projected goal $\Delta E/E < 0.5$ %
ToF resolution (FWHM):
$\Delta t < 100$ ps, projected goal $\Delta t < 50$ ps
In principle, these numbers are considered initial guidelines, while the actual LYCCA performance depends strongly on the available flight paths and experimental parameters, namely the mass regimes to be studied, secondary target thickness, or the focussing scheme of a relevant (Super-)FRS setting.

Section 2 details the various detector components of LYCCA. A brief description of the mechanical housing of the LYCCA wall ΔE-$E_{\rm res}$ telescopes in Sec. 3 is fol-

lowed by a brief overview of hitherto used processing and read-out electronics in Sec. 4. Section 5 illustrates very first in-beam commissioning spectra of LYCCA, thereby confirming the achievement of the design goals indicated above. The paper concludes with an outlook towards LYCCA as a FAIR-NUSTAR detection device.

2. The LYCCA Detector Components

2.1. The Target DSSSD

Double sided silicon strip detectors (DSSSD) are common in physics experiments as an apparatus to measure the energy loss, ΔE, and position, (x,y), of particles passing through the silicon bulk of the detectors. The silicon wafers used as LYCCA target DSSSDs are ion implanted, silicondioxide (SiO_2) passivated, and operated totally depleted with floating guard rings. They are obtained from RADCON Limited.

The nominally 300-320 μm thick wafers are square shaped, 60.1 mm $\times$60.1 mm in size with an active area of 58.5 mm $\times$58.5 mm. The active area is subdivided into 32 strips on both front (junction) p-side and rear (ohmic) n-side in orthogonal directions providing two dimensional position information. With 58.5 mm/32=1.83 mm, the pitch of the p-side strips is 1.80 mm with an interstrip SiO_2 isolation of 30 μm. To improve interstrip capacitive and resistive isolation from the adjacent n-strips on the ohmic side, a so-called p-type zone or p-stop structure surrounding n-strips was implanted. Thus the pitch size on the ohmic side is 1.63 mm with interstrip distances of 200 μm.

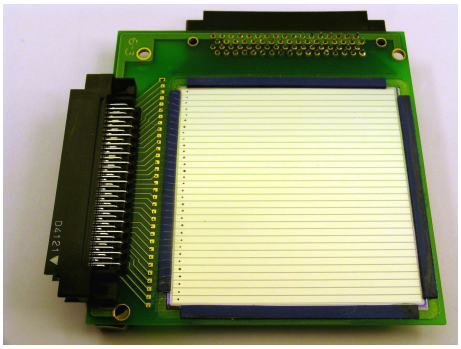

Figure 2: Photograph of a target DSSSD detector.

Leakage currents, upon delivery, range between 5-10 nA per strip with modest capacities of 33 pF per strip at full depletion voltage, which is typically reached at 50 V. The energy resolution and crosstalk was measured by scanning detectors with collimated ^{228}Th and ^{241}Am α-particle sources. A typical spectrum for this type of DSSSD, obtained in a test chamber using standard LYCCA vacuum feedthrough, cabling, and electronics (see Secs. 3 and 4), is shown in Fig. 5(a).

The thickness of the dead layers on both sides of detectors was determined by measuring the energy loss of the α particles by irradiating the detector from different incident angles. They are found to be $\sim$ 1.0 μm Si-equivalent on the junction side and $\sim$ 2.0 μm on the ohmic side. To optimize charge collection on the rear side of the detector the full depletion voltage was measured by injecting α particles into the ohmic side and maximizing detector response as a function of applied bias voltage.

The target DSSSD is mounted on a printed circuit board made of FR4 together with connectors and gold plated pads for strips bonding. Due to possible harsh radiation damage all components and material used for detector packaging allow temperature annealing at low-to-medium temperature for few days. The detector frame is mechanically compatible for mounting into the secondary reaction chamber together with the ToF Target detectors (cf. Secs. 2.3.2 and 2.3.3) and various secondary reaction targets.

2.2. The LYCCA ΔE-$E_{\rm res}$ Wall Telescope

The requirements described in Sec. 1 call for the use of telescopes based on segmented semiconductor detectors backed by segmented inorganic scintillators read-out by photodiodes (PD). Such a device presents a powerful tool for charged particle identification in a wide range of charge, mass, and energy, the latter if being used to stop the particles. Due to the very broad range of experimental conditions for which LYCCA is constructed, a modular design was deemed necessary.

All modules are identical telescopes where particle identification is obtained through ΔE-$E_{\rm res}$ measurements. In addition, internal segmentation of the telescope components provides the capability to sustain sufficiently high counting rates as well as multiple particle detection even within one single telescope. In the following subsections the design, construction, test results, and performance of LYCCA telescopes are presented.

2.2.1. The DSSSD Frame

For energy loss, ΔE, measurements, each LYCCA telescope comprises a 300-320 μm DSSSD as detailed in Sec. 2.1. To minimize physical dead areas surrounding each DSSSD, a very close packing of telescopes into the full LYCCA array is of high importance, thus a minimal amount of material for the DSSSD frame was a central design goal. The LYCCA solution is to mount

the silicon wafer into a thin frame made out of FR4 printed circuit board (PCB) material with the help of custom made tools and a bonding assembly [12] based on epoxy rubber CAF4 [13], which ensures the necessary mechanical stability and elasticity for possible mechanical tensions on the frames. Only 0.2 mm of the detector frame extends beyond the wafer on the two connector free sides, and 2.0 mm on the two sides where signal multipin connectors are mounted. The frame has gold plated pads for bonding and pin-like connectors (BLX-1-056-40G) soldered for signal extraction.

The challenge of minimal dead space of the telescope front face and signal read-out combined with mechanical stability for the subsequent heavy-weight block of CsI(Tl) scintillators (see below) is overcome by specially designed signal transportation boards. These boards fabricated out of FR4 PCB material are equipped at one edge with connectors (SLX-1-053-30G) to be attached to the thin DSSSD frame. At the another end of the signal transportation board multipin connectors (KEL 8831E-068-170) are mounted for further DSSSD signal transportation towards the feedthrough boards of the LYCCA vacuum chamber. A closeup view of a DSSSD mounted on its PCB frame and in combination with the signal transportation boards assembly is shown in Figs. 3(a) and (b), respectively.

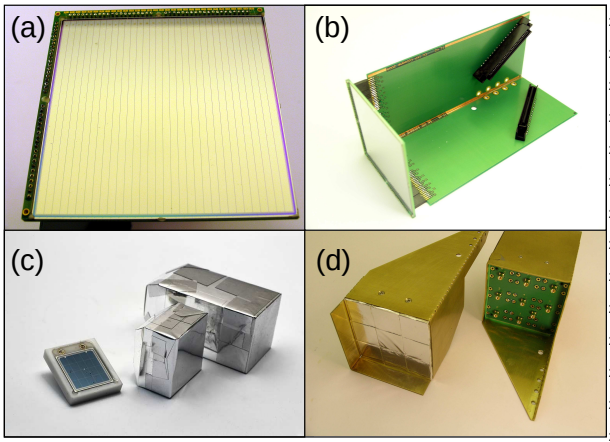

Figure 3: LYCCA module elements: (a) A DSSSD wafer mounted in its thin PCB frame and (b) coupled to the signal transport boards. (c) A photodiode mounted in its ceramic plate and CsI 'short' and 'long' crystals wrapped in the ESR reflecting foil. (d) A 9-element CsI-block in the brass frame.

2.2.2. The CsI Block

Each LYCCA telescope is equipped with an array of nine CsI(Tl) crystals being placed 10 mm behind the DSSSD wafer to measure the full residual energy, $E_{\rm res}$, of the particles. The front face of all CsI(Tl) crystals has the dimension 19.4×19.4 mm^2 and there are two different lengths of crystals available: a 'long' version of 33.0 mm in depth plus 7.0 mm of pyramidal lightguide and a 'short' version of 10.0 mm in depth with 5.0 mm pyramidal lightguide. The dimensions of the back end of the pyramidal light guide are 10.4×10.4 mm^2 matching the size of the read-out PDs.

The choice of CsI(Tl) is dictated by its high stopping power, high light output, and the relatively easy handling of this type of inorganic scintillator. One of the important characteristic of the CsI(Tl) crystal for high-resolution charged-particle spectroscopy is light output variations arising from possible gradients or local fluctuations of the Tl concentration. To achieve optimal light uniformity all crystals were machined from a single ingot. The typical Tl concentration is 0.08-0.10 mol%. All crystals were supplied by Amcrys-H Ltd., Kharkov, Ukraine [14].

The achievable resolution of total energy measurement depends first of all on non-uniformities of light collection across the active volume of a CsI crystal. Secondly, it depends on the position of energy deposition but also on the deposited energy density. Such aspects are detailed in Refs. [15, 16, 17]. For example, light output depends strongly upon the reflecting material used for wrapping. ESR film was proposed [18] and also tested for LYCCA and found to be most optimal for wrapping all sides of the crystals except for the front face. The ESR foil is partially transparent in the blue region of scintillation light. To achieve optical isolation of a crystal from its neighbours each crystal was additionally wrapped into 12μm thin Al-foil. The same foil was used to cover front face of the crystal to maximize light collection from the scintillation process and at the same time minimize dead layer for incoming particles. Following a number of cross checks, no additional lapping to compensate for potential light non-uniformity along the crystals appears needed, not least due to the relatively small dimensions of the LYCCA CsI(Tl) crystals.

The scintillation light produced in the CsI(Tl) crystals is read-out by photodiodes (PD). The PDs are 10.6 mm $\times$11.6 mm $\times$0.3 mm in size and supplied by RADCON Ltd., Zelenograd, Russia. The PDs are mounted into custom-made application specific ceramic frames and glued directly onto the light guide of the crystal by means of Epo-Tek 302 optical epoxy. The chosen PD has a very good matching for the CsI(Tl) scintillator emission light: the quantum efficiency is as high as $\sim$ 82-86% at 560 nm, which is the peak position in the emission spectrum of the CsI(Tl). The total spectral response of the PD ranges from 320 nm up to

1060 nm with a maximum at some 920 nm. At nominal operating voltage 35 V the leakage current is on the level of 1-2 nA and the capacitance is 38-40 pF at full depletion.

Nine CsI(Tl)-PD units are packed into a 3×3 array into a brass frame which allows for proper relative alignment of all active elements of a LYCCA telescope (see below). A FR4 PCB CsI(Tl)-PD signal distribution board is soldered directly onto the nine PD's pins. This board is also equipped with MMCX connectors, and shielded coaxial cables are used for PD signal transportation towards the feedthrough boards of the LYCCA vacuum chamber to guarantee noise immunity and negligible signal cross talk. Figs. 3(c) and (d) provide photographs of various CsI(Tl) detector components.

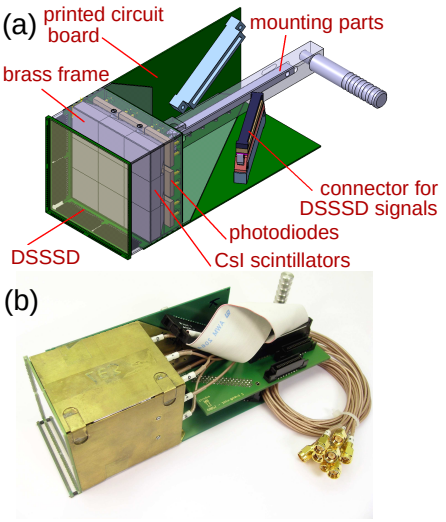

Figure 4: A LYCCA telescope (a) in its three-dimensional CAD drawing stage and (b) in its LYCCA-1 realization.

2.2.3. The LYCCA Module

The single LYCCA telescope module is made up of one DSSSD mounted on its thin frame connected to the signal transportation boards, with the brass frame of a CsI scintillator block mechanically attached. Additionally, a custom-made mechanical locking system for mounting the telescope into LYCCA chamber (see Sec. 3) is linked to the brass frame and the signal transportation boards. The detachable nature of the CsI block allows easy access to both telescope components and active elements for exchange, service or repair. Figs. 4(a) and (b) provide both the technical drawing and a photograph of a real LYCCA telescope.

2.2.4. Bench Tests

A test vacuum chamber has been configured to enable high-resolution test measurements and overall performance tests for LYCCA detectors. The test chamber is equipped with mechanics, cables, connectors and front-end electronics identical to items used in the real LYCCA chamber. Various radioactive sources can be mounted inside the chamber to provide possibilities for comprehensive detector testing.

The energy resolution and crosstalk for each DSSSD was measured by scanning detectors with collimated ^{228}Th and ^{241}Am α-particle sources in the test chamber. A typical spectrum, obtained using standard LYCCA electronics (cf. Sec. 4), vacuum feedthrough and cabling is provided in Fig. 5(a). The pixel resolution has a typical value of less than 50 keV FWHM at 9 MeV α energy, which comprises also significant uncertainties from source as well as deadlayer thicknesses.

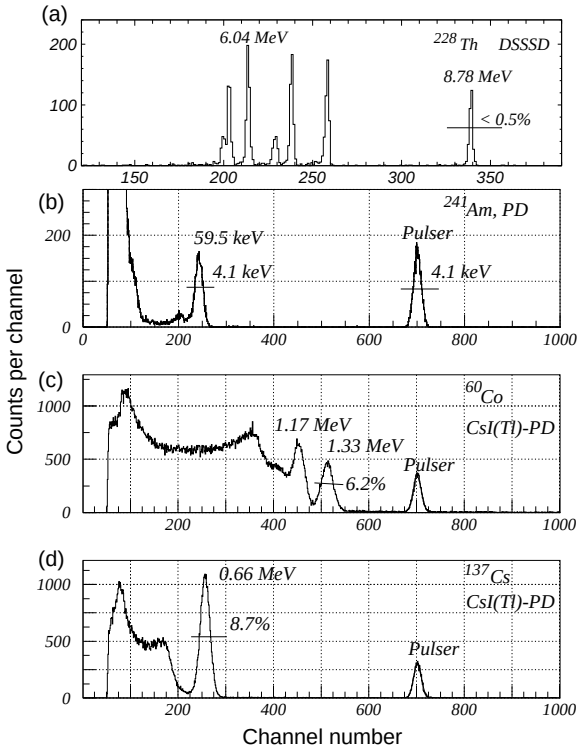

Figure 5: Energy calibration spectra for a bare photodiode (b), a CsI(Tl)-PD detector (b,c), and a LYCCA DSSSD detector (d). Energy resolutions are indicated and there are labels for the respective radioactive source used.

Standard γ-ray sources (^{60}Co, ^{137}Cs, ^{243}Am) have been used for various energy resolution measurements of bare photodiodes, single CsI(Tl)-PD units, and complete CsI block assemblies, respectively. Figs. 5(b)-(d) show some of these γ-ray spectra. For example, the

energy resolution measured at $E\gamma$ = 1.3 MeV yields 6.2% FWHM for the 'short' crystal version. Taking into account the well known $R \sim 1/\sqrt{E}$ power law relation for energy resolution dominated by statistical effects one can anticipate that the projected goal is easily reached for an expected minimum deposited energy of at least several GeV in CsI(Tl) crystals in real PRESPEC or HISPEC experiments. Following the modules' use in real experiments, spectra such as those displayed in Fig. 5 serve as reference spectra for quality assessment and maintenance procedures [19].

Successful tests of the first LYCCA prototype telescope inside the test chamber performed with a proton beam delivered by the Tandem Accelerator of the University of Cologne are summarized in Ref. [20].

Further calibration aspects for ΔE-$E_{\rm res}$ telescopes are addressed in Refs. [21, 22] followed by in-beam tests during the R&D phase of related DSSSD-CsI(Tl) telescope arrangements [23].

2.3. The LYCCA ToF Detectors

The R&D of LYCCA ToF detectors has followed essentially two lines (cf. Ref. [11]): A new class of large-area scintillation membranes [24] and the development of polycrystalline, chemical vapour deposited diamond detector wafers [25]. In-beam commissioning experiments have been successfully performed with both systems, while availability, performance, and also cost-per-performance issues favour the scintillator concept, at least within the LYCCA framework.

2.3.1. The ToF Start and ToF Stop Elements

The ToF Start and ToF Stop detectors follow a new design approach for large-area plastic scintillation detectors: A circular membrane of Saint-Gobain BC-420 with 27 cm diameter is read out by 32 Hamamatsu R7400U photomultiplier tubes. The R&D, components, construction, and the in-beam result of an intrinsic detector resolution of $\Delta t \ll 50$ ps FWHM is detailed in Ref. [24]. In brief, the unusually good timing resolution for plastic scintillator systems is achieved through collecting the light in 32 independent measurements. Taking an average, i.e. to first order by means of the factor $1/\sqrt{32} \sim 0.2$, results in a better effective ToF resolution than other fast materials with a better intrinsic resolution such as, for example, diamond detectors.

2.3.2. The ToF Target Scintillation Detector

Based on the achievements of the large membrane scintillators, a smaller Target ToF scintillation detector with an active diameter of 73 mm has been designed and built recently. This dimension follows (*i*) the need for typical beam spot sizes of relativistic radioactive ion beams at the secondary target position, namely $\sigma_x \sim \sigma_y \sim 1.5$ cm, and (*ii*) the constraints by the size of the HISPEC-AGATA vacuum chamber surrounding the secondary target. Figure 6 provides a drawing and photograph of this detector. Simulations based on the studies in Refs. [24, 26] indicate that despite the necessarily smaller number of only 12 photomultiplier tubes a time resolution similar to the above can be achieved by using quenched Saint-Gobain BC422Q(0.2%) instead of BC-420 and by replacing the former Hamamatsu R7400U tubes with the latest generation of Hamamatsu R9880-210. A detailed performance characterisation of this new detector is going to be a part of a comprehensive subsequent publication on LYCCA in-beam measurements [27].

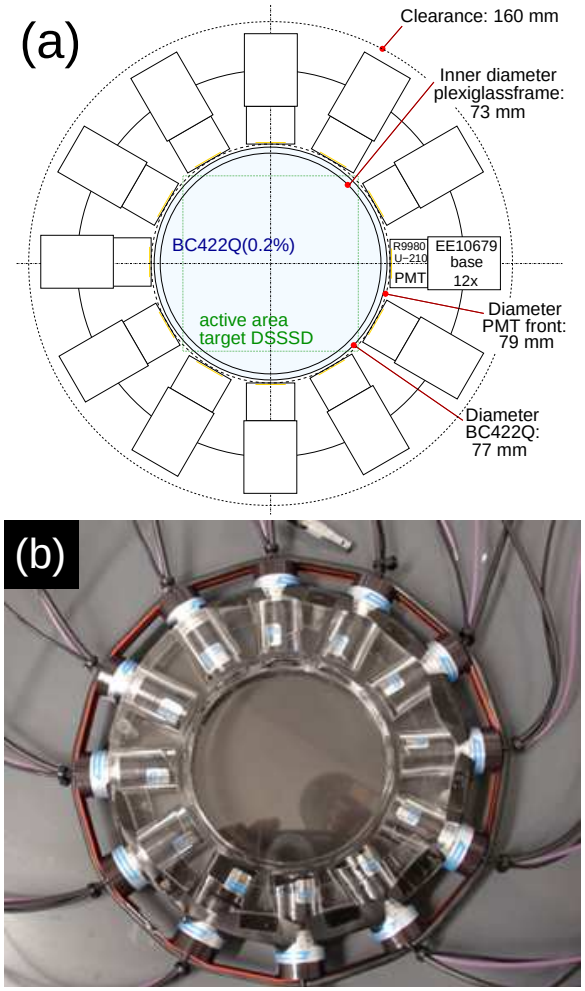

Figure 6: (a) Drawing of the LYCCA ToF Target detector and (b) photograph of its realization.

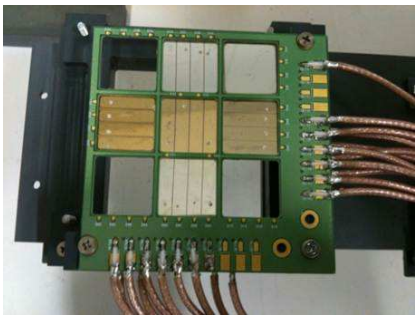

Figure 7: Photograph of the prototype of the LYCCA Target ToF diamond detector.

2.3.3. The ToF Target Diamond Detector

Any LYCCA ToF detector placed at the target position is required to cover the full area of the secondary target. This necessity led to the development of what we believe to be one of the largest area diamond detectors tested to date. As can be seen in figure 7, the detector can accommodate nine $20\times20\times0.3\,\mathrm{mm}^3$ polycrystalline diamond wafers formed by chemical vapour deposition, although only six were used for this experiment. Five of the wafers are segmented into four strips measuring 18×4.5 mm^2. These wafers were mounted onto a custom-made PCB, allowing for separate biasing and signal extraction for each strip. The signals were amplified using 2.3 GHz broadband DBAIV preamplifiers [28], specially designed for fast pulses from diamond. Further details on the fabrication and development results from an earlier version of this diamond detector can be found in Ref. [25].

In-beam measurements were made with the large-area plastic start and stop scintillators, as well as the target diamond detector to enable detailed comparisons of their timing performance. The precision of the diamond - plastic stop ToF measurements were compared with the plastic start - plastic stop ToF measurements, which had flight paths of $d_{\mathrm{out}} = 3.61(1)$ m and $d_{\mathrm{tot}} = 4.31(3)$ m, repectively. Details of the latter can be found in Sec. 5. The same procedure applied to the diamond indicates a resolution of 193 ps (FWHM). This compares with the best result of 103 ps (FWHM), obtained at Texas A&M University [25] using the same configuration of diamond wafer.

Further analysis has concluded that this worsening of the resolution is likely to be caused by the necessarily large length of cable (2.5 m compared with 1 m at Texas A&M University) present between the diamond detector and the DBAIV, which significantly increased the capacitance on the input of the preamplifier. The charge collection from the detector was also found to be smaller during the commissioning experiment. These factors would be expected to have adverse effects on the noise contribution to the final amplified signal, and the timing resolution would become worse as a result. Indeed, it should be noted that where diamond has demonstrated especially good timing resolution, the custom built electronics have always been adjacent to the detector [29].

From this is can be concluded that it will be challenging for diamond to meet the optimum resolution required for LYCCA without significant redesign of the signal processing arrangements. This, coupled to the better final resolution demonstrated by the the plastic scintillators (cf. Sec. 5) has led the LYCCA collaboration to decide that the LYCCA ToF measurements for the final NUSTAR device should be undertaken using the plastic scintillation detectors.

3. The LYCCA Chamber

The mechanical construction to hold the LYCCA ΔE-E_{res} modules (see Sec. 2.2.3 and Fig. 8(a)) is compatible with the final full LYCCA setup and flexible to be placed at any suitable position along the Super-FRS and HISPEC beamlines, provided rather trivial coupling flanges being manufactured in the future. In addition, the mechanical construction allows for a relatively easy replacement of single LYCCA ΔE-E_{res} modules if deemed necessary from an experimental point of view.

The LYCCA-chamber itself is based on a cylindrical vacuum vessel with a diameter of 800 mm and a depth of 400 mm. The upstream side has an open circular entrance with a diameter of 450 mm for the incoming particles. The vacuum chamber is designed to host up to the anticipated 26 LYCCA ΔE-E_{res} detector modules in 5 rows of 4, 6, 6, 6, and 4 modules each. The photograph on the right hand side of Fig. 8 shows the realization of the LYCCA vacuum chamber with 3×4 LYCCA modules mounted. This represents the configuration used for the first PRESPEC experiments in 2010 and 2011. For the PRESPEC-AGATA experiments in 2012 and 2014, 4 additional modules were implemented, namely 2 in the centre of the top and 2 in the bottom row, respectively.

While fixed on top of a support table, the LYCCA vacuum vessel has a standard flange to connect to a vacuum pumping system at its bottom. Radially, some 70 vacuum feedthroughs are foreseen to carry the signals from detector elements inside the vacuum chamber into custom-made 32-channel preamplifiers (cf. Sec. 4.2) via glued-in printed circuit boards. Until 2014, this scheme is followed for both CsI and DSSSD detectors

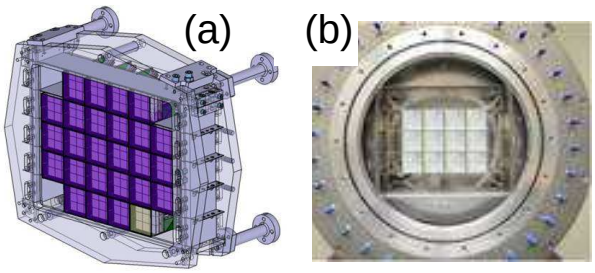

Figure 8: (a) Technical 3D drawing of the holding structure for LYCCA modules inside the LYCCA Wall vacuum chamber. (b) Photograph of the LYCCA Wall vacuum chamber as seen by the beam with twelve LYCCA modules mounted inside the holding structure.

(cf. Secs. 4 and 5). The preamplifiers connect via 68-pin high-density connectors and are mechanically oriented and held in place by means of a dedicated 'plug-and-play' mechanism. Hence, both electrical contacts and mechanical stability are secured while keeping the distance between detectors and preamplification stage minimal. Vacuum feedthroughs are also provided for temperature and pressure read-out.

For the complete PRESPEC experimental campaign 2010-2014, the LYCCA ToF Stop detector (cf. Sec. 2.3) is also contained in the main LYCCA Wall vacuum chamber. In fact, some of its signal- and high-voltage vacuum feedtroughs can be seen in Fig. 8(b). For HISPEC, a revised and further optimized LYCCA ToF Stop plastic scintillation detector, covering the complete area of all 26 ΔE-E_{res} modules, is being manufactured. This detector is going to be inside a separate vacuum housing in front of the existing LYCCA Wall vacuum chamber.

More comprehensive information on the LYCCA vacuum chamber is provided in Refs. [11, 20, 30, 31].

4. LYCCA Electronics

4.1. Processing of LYCCA ToF Detector Signals

The processing of the signals of the photomultiplier tubes of the LYCCA ToF system based on plastic scintillators is detailed in Ref. [24]. In short, the outputs of the photomultiplier bases are directly plugged into 5-channel Phillips Scientific Model 715 constant fraction discriminators [32]. Commercial time-to-digital converters CAEN V1290A, providing 21-bit dynamic range and 25-ps time bins, are used to digitize the individual timing signal with respect to a common reference, namely the accepted event trigger signal of the complete PRESPEC data acquisition system. Once in place, the 12 timing signals of the Target ToF detector are also put into a logic OR unit to provide an optional 'Target ToF' trigger input signal. The remotely controllable high-voltage supply to the photomultiplier bases comprises four 16-channel ISEG EH160-30n305SHV modules in a common main frame [33].

A similar electronics scheme was also used for the target diamond detector. The outputs of the DBAIV preamplifiers were fed into Phillips Scientific Model 708 leading edge discriminators [32], and then converted into ECL signals and passed into the same CAEN V1290A TDC. Each strip on the diamond detector was biased to 395 V, which was applied via the DBAIV preamplifiers. Further details can be found in Ref. [25].

4.2. The 32-channel LYCCA preamplifier

Within the framework of the LYCCA project, the CSP-32(X) series of highly compact, charge-sensitive preamplifiers was developed at the University of Cologne. The underlying design is such that in principle a wide energy range of the signals from both DSSSDs and PDs is covered, with an easily reconfigurable amplification stage up to a 10 GeV range. For LYCCA the model CSP-32(4.1GeV) is selected from this series [11], which foresees a switchable dynamic range between 1.3 GeV and 4.1 GeV. An overview of the main components of the CSP-32(4.1GeV) is presented in Fig. 9. It consists of the following stages:

- a charge-sensitive loop with frequency compensations,
- a passive pole-zero cancellation and attenuation stage, and
- a balanced differential output buffer.

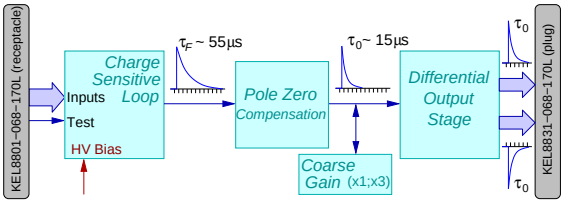

Figure 9: Block diagram of one channel of the front-end electronics for DSSSD and photodiode processing of LYCCA modules. Fall times of $\tau_F \sim 55\ \mu$s after the first amplification stage and $\tau_0 \sim 15\ \mu$s following pole zero compensation are indicated.

The charge sensitive loop has a conversion factor of 50 pC/V. It comprises an input stage with a very low noise jFET transistor, a current feedback operational amplifier, a passive feedback circuitry and a rather complex frequency compensation network. The use of a large feedback capacitance was mandatory to achieve

the large dynamic range but moreover to account for placement of the detectors in a relatively large reaction chamber, which implies long wiring between detector elements and the charge sensitive preamplifier input circuitry. In order to cope with these adverse conditions and to get a transfer function with a flat amplitude response at the highest possible bandwidth, a multiple frequency compensation network was designed and implemented.

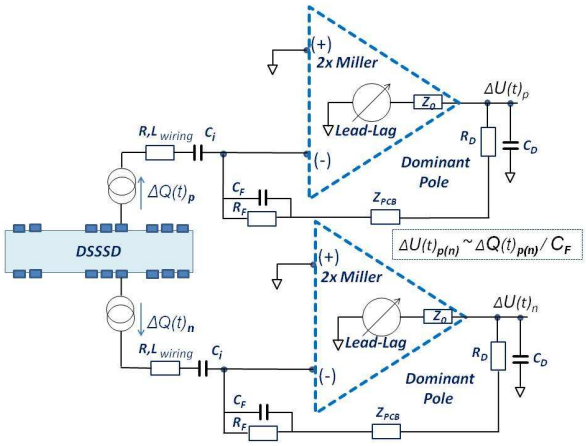

Figure 10: Simplified block diagram of the equivalent transimpedance amplifier stages and frequency compensation networks.

The connection of the detector elements to the charge-sensitive loop input stage is AC (10 nF/400 V). This is imposed by the required detector bias voltage of up to 200 V. The choice of the preamplifier input jFET type is one critical issue of such developments. After some tests performed, we have found that the n-channel jFET models BF861A and BF861C manufactured by NXP Semiconductor represent the most adequate choice. In fact, both provide a very low-noise with a working point at a drain voltage of only $\sim$ 2.0-2.5 V and a drain current of less than 4 mA, i.e. a power consumption of only $\sim$ 8-10 mW.

The transimpedance amplifier of the charge sensitive loop is built around a miniature current feedback operational amplifier (AD8005ART; RT-5 package) which is showing a wide signal bandwidth (270 MHz), very low quiescent current (typically 400 μA) and at the same time very low input voltage noise (4.0 nV/ $\sqrt{\text{Hz}}$ at 10 MHz). To match the different detector requirements the feedback network values can vary for different configurations: For LYCCA DSSSD detectors, the default values are C_F = 56 pF and R_L = 10 MΩ, respectively τ_F $\sim$56 μs (Fig. 9).

The frequency compensation circuit is implemented in the charge sensitive loop and it is similar to the AGATA FEE design [34]. It comprises three main components, namely one high-pass filter (as the Miller effect like internal compensations of the equivalent operational amplifiers), one lead-lag filter, and finally one dominant-pole compensation circuit. The lead-lag compensation with a time constant of $\sim$ 3-5 ns is a rather high frequency compensation without sacrificing the close-loop gain performance.

The dominant pole frequency compensation circuit detailed in Fig. 10 compensates the pole existing in the more complex feedback network of the charge sensitive stage [35]. One takes advantage of the very large open loop gain of the charge sensitive stage and its quite small output impedance, Z_0, capable to drive the rather large output capacitor of 10-20 pF. This network has a time constant of $\sim$ 1.0-1.5 ns and acts efficiently as a dominant pole compensation without causing instabilities in interaction with the intrinsic equivalent operational amplifier pole.

The rise time, t_{rise}, of the charge sensitive stage is $\sim$ 13 ns for zero input capacitance, C_{in} = 0 pF, with the rise-time slope being 0.3 ns/pF with almost no overshoot or undershoot over the whole dynamic range. A typical transfer function in time domain for C_{in} $\sim$ 60 pF and a step function as input test signal with t_{rise} $\sim$ 1 ns is shown in Fig. 11(a).

To obtain similar fall-time characteristics of the output signals for different dynamic range configurations of the CSP-32(X) series, a pole-zero cancellation network is also required, as shown in Fig. 9. By default the fall time of the output signals is $\sim$ 15 μs.

A differential signal transmission mode is chosen to enhance the rejection to common-mode noise and potential disturbances picked up along the output cable. A balanced differential output stage has been designed around the AD8012AR dual operational amplifier which features low noise, low power, and wide bandwidth. Only ±6 V power supply has been chosen due to the overall power consumption limitation of the 32 channels packed in a relatively small metal case of 80 mm ×40 mm ×120 mm in size. A photograph of an open case is provided in Fig. 11(b).

The main specifications of the CSP-32(4.1GeV) can be summarized as follows:

- conversion gain of the CSP stage 800 mV/GeV(Si),
- noise $\sim$ 2.8 keV FWHM (C_{detector} $\sim$ 0 pF),
- noise slope 11 eV/pF,

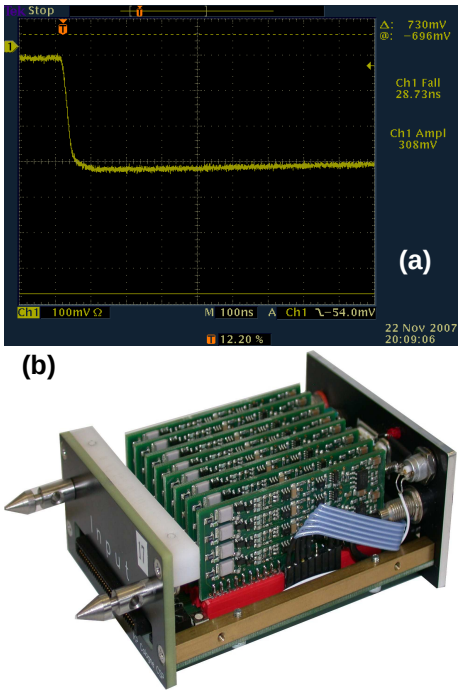

Figure 11: (a) Transfer function in time domain for a test with a step function as input signal with $t_{rise} \sim 1$ ns. (b) View of the CSP-32 charge-sensitive preamplifier (box opened). 8 boards are visible, each equipped with 4 channels.

- rise time ∼ 10 ns,
- rise-time slope 0.3 ns/pF,
- fall time ∼ 15 μs by default, while it can optionally be factory adjusted in the range of 10-50 μs,
- a switchable coarse gain of 1/1 or 1/3 is implemented,
- differential output signals (with 100 Ω differential output impedance and a dynamic range of ± 4.5 V-terminated, here corresponding to the 4.1 GeV range),
- overshoots/undershoots less than 2.5% over the whole dynamic range.
- the 32 output signals can be directly digitized with two GSI-EE 16-channel FEBEX3 sampling ADC modules [38]

Last but not least, cross talk between detector channels has to be considered in a complex detector system where the sensor itself is highly segmented. Special care has been taken to minimize the cross talk between segments and between detectors at the level of the reaction chamber ensemble set-up. To avoid additional crosstalk between LYCCA detector elements, separated return ground paths for each individual segment are provided, while the inductivities to the segment electrode within the detectors wiring cannot be omitted.

4.3. Processing of LYCCA DSSSD and CsI Elements

Until the final LYCCA read-out scheme based on highly integrated and fully digitized preamplifier signals [11] becomes operational within the FAIR-NUSTAR data acquistion environment, an intermediate path based on readily available and reasonably affordable integrated electronics modules has been followed.

Each of the 32 signals from the p-side and the n-side of the Target DSSSD are handled by one 32-channel preamplifier box described in the previous Sec. 4.2. Sixteen channels of differential preamplifier output are carried by shielded twisted pair cable towards a total of four single-unit NIM, 16-channel analogue shapers of type Mesytec STM16 or MSCF16 [36]. The in total 64 energy channels are subsequently digitized by two CAEN 785 peak-sensing analogue-to-digital converters (ADC), the corresponding times of the 32 p-side channels measured by a CAEN 775 time-to-digital converter (TDC) relative to the accepted event trigger. A logic OR of all 64 timing channels can be used as an optional 'Target DSSSD' trigger input signal.

During the 2010-2011 PRESPEC experimental campaign the four DSSSDs in the centre row of LYCCA modules [cf. Fig. 8(b)] were processed in an almost identical fashion: 8 custom-made preamplifiers (cf. Sec. 4.2), hence 16 analogue shapers coupled to 8 ADCs were used, while the 128 timing signals of the p-sides were digitized by a 128-channel CAEN 767 TDC. The signals of the remaining 8 DSSSDs were combined in units of four strips inside the LYCCA vacuum chamber, which gives rise to additional 8*(32+32)/4=128 silicon channels, i.e. four more preamplifiers, eight more analogue shapers, four more ADCs, as well as a second CAEN 767 TDC.

During the 2012-2014 PRESPEC-AGATA experimental campaign, a total of 16 LYCCA ΔE-$E_{\rm res}$ modules are in use. Here, two neighbouring signals of all DSSSDs are joined inside the LYCCA vacuum chamber, which yields a total of 16*(32+32)/2=512 silicon channels. These 512 channels are handled by 16 preamplifiers, 32 analogue shapers, 16 ADCs, and two CAEN 767 TDCs, since still only the times of the p-sides of the DSSSDs are being recorded. In both configurations, a logic OR of all DSSSD p-side timing channels could or

can be used as an optional 'Wall DSSSD' trigger input signal.

The photodiode read-out of the CsI detectors in the LYCCA modules is handled very similarly: The modules are grouped together in units of three, such that 3*9=27 photodiodes can be processed by one 32-channel preamplifier (identical to the one used for the DSSSDs, cf. Sec. 4.2), two analogue shapers, one ADC, and 32 channels of either a CAEN 775 TDC or part of a CAEN 767 TDC. A logic OR of all timing signals could or can be used as an optional 'Wall CsI' trigger input signal.

The high-voltage bias supply to both DSSSDs and photodiodes is provided by a set of four 4-channel Mesytec MHV4 NIM modules [36]. Remote control of MHV4 voltages as well as STM16/MSCF16 gain and threshold settings are enabled by two Mesytec MRC1 slow-control units [36].

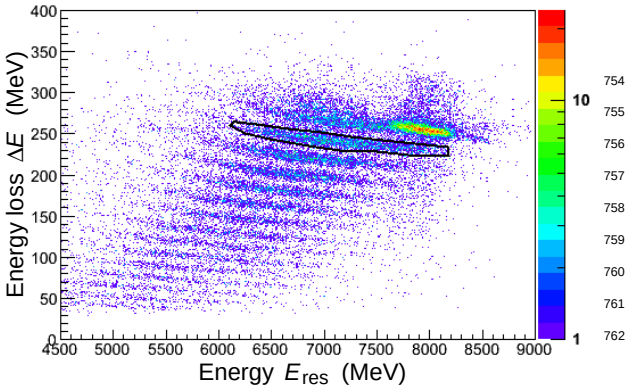

Figure 12: Energy loss vs. energy plot showing the Z distribution measured in one LYCCA ΔE-E_{res} module. The $Z = 26$ selection for Fe fragments is shown.

5. First In-beam Commissioning Results

The first in-beam commissioning experiment for LYCCA took place in September 2010, which aimed to determine the performance of the LYCCA detectors for nuclei around $A \sim 60$. A 550 MeV/u ^{64}Ni beam was incident upon a 4 g/cm^2 thick ^{9}Be production target at the entrance window to the FRS [6]. A secondary beam of ^{63}Co was selected and allowed to pass through a number of FRS detectors, the LYCCA ToF start scintillator and the LYCCA target detectors, which consistet of the target diamond prototype detector and a DSSSD. A 0.4 g/cm^2 thick ^{197}Au secondary target followed these detectors. The energy of the ^{63}Co beam at this point was approximately 165 MeV/u. The beam continued to pass through the remaining LYCCA ToF Stop scintillator and LYCCA telescopes before coming to rest in the LYCCA wall CsI detectors. The flight distances (cf. Fig. 1) were $d_{\mathrm{in}} = 700(5)$ mm and $d_{\mathrm{out}} = 3.61(1)$ m.

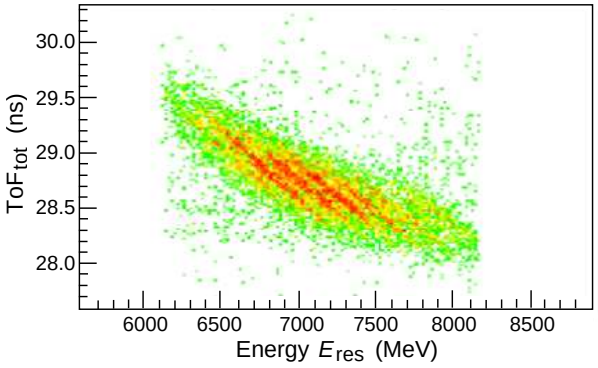

Figure 13: ToF$_{\mathrm{tot}}$ vs. energy E_{res} plot showing Fe fragments from the commissioning data.

In order to get an idea of the performance of LYCCA, the mass resolution of Fe fragments, primarily produced by secondary beam interactions with the diamond detector and DSSSD at the target position, was evaluated. Using this measurement and knowledge of the energy resolution, the timing resolution was extracted and all resolution values were compared with those used in the LYCCA simulations [10] and outlined in the LYCCA TDR [11].

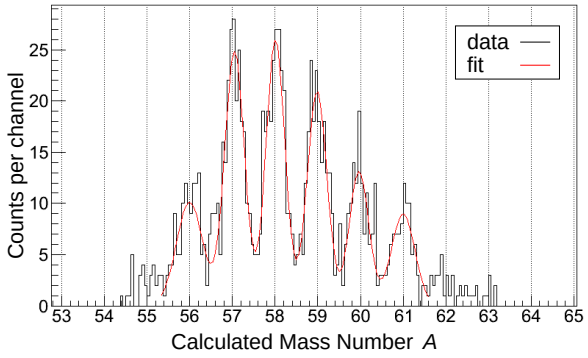

Figure 14: Fe fragment masses calculated on an event-by-event basis. The mass resolution of $\Delta A = 0.55$ (FWHM) was determined from the average width of the six peak Gaussian least sqaures fit shown.

A $Z = 26$ selection was made using $\Delta E - E_{\mathrm{res}}$ data from the LYCCA wall DSSSDs and CsI detectors respectively, as can be seen in Fig. 12. Isotopic identification of the Fe fragments could then be provided by

the $\mathrm{ToF_{tot}}$ measurements between LYCCA start and stop scintillators, as well as the E_{res} measurements from the LYCCA wall detectors. Only one central ΔE-E_{res} wall module was used throughout the analysis to guarantee that partially insufficient calibration data did not compromise the mass resolution measurements. Projectile tracking using the target and wall DSSSDs allowed position corrections to be made to the LYCCA scintillators, which improved the accuracy of the timing measurements [24].

The resulting $\mathrm{ToF_{tot}}$ vs. E_{res} histogram is shown in Fig. 13, and can be compared with the simulated plot for fragments ^{50}Fe to ^{53}Fe in Ref. [10], i.e. in a similar Z and A regime and comparable particle energies and flight distances. At least four Fe isotopes can be identified from the experimental data in Fig. 13. The separation between neighbouring 'diagonal lines', i.e. neighbouring isotopes, is topologically very similar to expectations from the simulations in Ref. [10].

The time-of-flight between the target and the LYCCA wall, $\mathrm{ToF_{out}}$, and total energy measurements were used to calculate fragment masses on an event-by-event basis. $\mathrm{ToF_{out}}$ was determined from $\mathrm{ToF_{tot}}$ using knowledge of the beam velocity β at various points along the beamline, and LYCCA tracking information was used to correct for different particle trajectories along the flight path. The total energy measurement also required correction to ensure that energy losses in the stop scintillator and the shielding foil were taken into consideration.

The result of these calculations for the $Z = 26$ selection can be seen in Fig. 14, which also includes a restrictive gate on incoming fragments from the FRS. An average measurement of the six most prominent peaks produced a mass resolution of $\Delta A = 0.55(3)$ (FWHM). A timing resolution for the LYCCA ToF system could only be determined by working backwards from this mass resolution and taking a known energy resolution, which was measured using a ^{64}Ni beam with minimal matter in the FRS beamline. This reduced the energy straggling of the beam, allowing an upper limit of 0.69(2) % (FWHM) to be assigned to the energy resolution. With this knowledge, a lower limit to the effective timing resolution of $\Delta t = 72(4)$ ps (FWHM) was extracted for the LYCCA timing system, which corresponds to $\Delta t = 51(3)$ ps (FWHM) for each timing detector. Due to coarse position corrections in the present analysis and additional energy and position straggling of the ^{63}Co fragmentation beam, this number is about a factor of two worse compared to the number achieved in a dedicated test with a primary ^{64}Ni beam in Ref. [24]. Nevertheless, it still suffices for proper mass resolution (cf. Fig. 14). More details of the analysis procedure of this commissioning experiment are presented in Ref. [37].

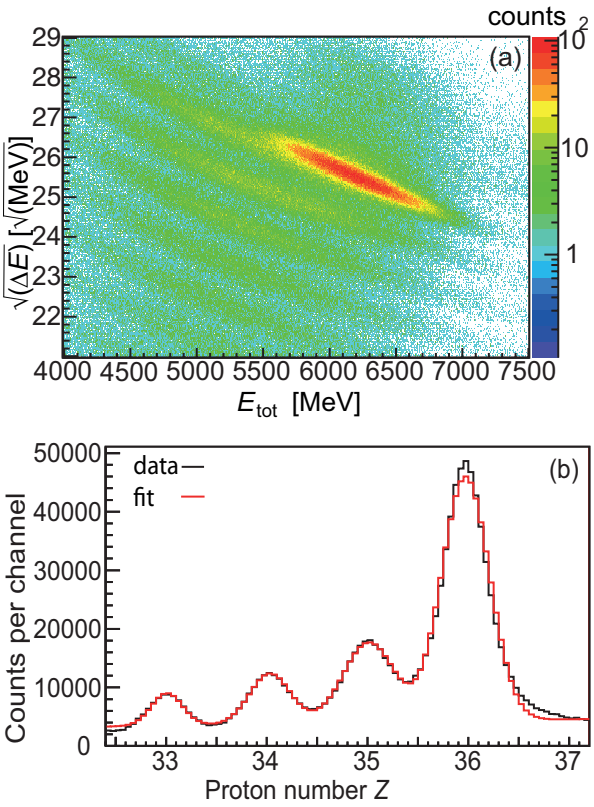

Figure 15: (a) LYCCA $\sqrt{\Delta E}$ - E_{tot} plot and (b) charge Z distribution derived from the energy loss ΔE after the secondary target for the ^{84}Kr fission fragment beam.

In another experiment, a secondary ^{84}Kr beam was produced by relativistic fission of a ^{238}U primary beam at 650 MeV/u on a ^{9}Be target. This FRS setting on stable ^{84}Kr was chosen for calibration purposes prior to a Coulomb excitation experiment of the unstable isotope ^{88}Kr. The experimental set-up was identical to the one of the ^{63}Co test experiment described above, but with one exception: the prototype diamond ToF detector element was removed.

In Fig. 15(a) the square root of the energy loss in the DSSSD $\sqrt{\Delta E}$ is plotted versus the total kinetic energy E_{tot} deduced from the sum of the energy loss ΔE in the DSSSD and the energy E_{res} deposited in the CsI. The different nuclear charges from bare ions after the secondary target are clearly separated in this plot. Figure 15(b) shows the Z distribution obtained from ΔE after applying a momentum correction and a Z calibration (for more details see Ref. [30]) together with a least-square fitted multiple gaussian function. From this fit

the charge resolution is calculated to be $\Delta Z = 0.55$.

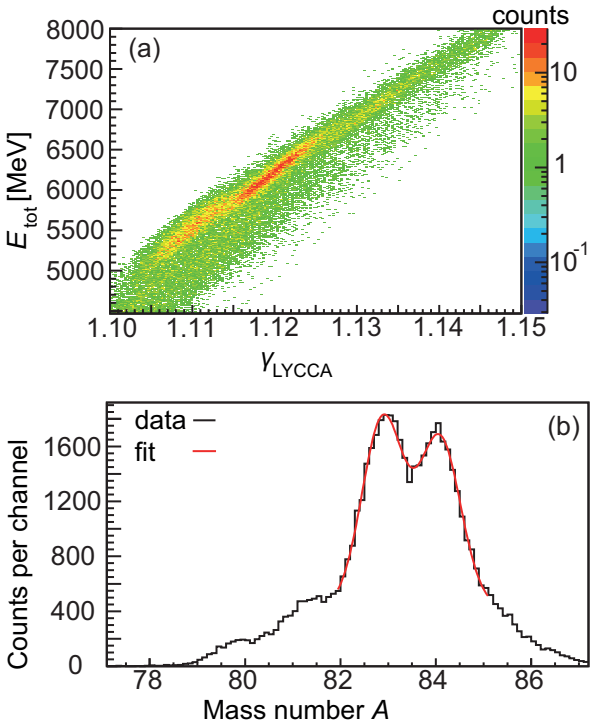

Figure 16: (a) LYCCA E_{tot} versus γ_{LYCCA} plot and (b) mass A distribution obtained from the distribution (a) by applying a momentum correction, a calibration, and background subtraction. Both plots are in prompt coincidence with incoming $Z = 35$ fragments using the preceding FRS ion identification.

Masses are determined from the correlation between total kinetic energy and the time-of-flight. Figure 16(a) shows the mass identification plot E_{tot} versus γ_{LYCCA}. The relativistic Lorentz factor γ_{LYCCA} is calculated from the ToF measured with LYCCA after the secondary target. As a by-product of the ^{84}Kr beam also bromine isotopes can be selected from the incoming beam cocktail with a gate on $Z = 35$ imposed on the FRS ion identification. Following a $Z = 35$ selection in LYCCA as well, the capability of LYCCA to separate the different Br isotopes after the secondary target is demonstrated. The two-dimensional distribution displayed in Fig. 16(a) is transformed into the mass spectrum shown in Fig. 16(b) by employing a momentum correction, a mass calibration, and subtraction of background. For a detailed description see Ref. [30]. The distribution is least-squares fitted with a multiple gaussian function with equal width values. The resulting mass resolution (FWHM) for masses $A \sim$ 80-85 yield $\Delta A = 1.02$.

The preceding – and to some extent still preliminary – analyses provide the proof-of-principle of the LYCCA detection scheme. Both energy and timing resolutions of the various LYCCA detector elements have to work according to or even better than specifications to achieve the main characteristics of the set-up, namely

- $\Delta Z/Z \lesssim 0.022$ ($Z \lesssim 26$).
- $\Delta Z/Z \lesssim 0.015$ ($Z \lesssim 36$).
- $\Delta A/A \lesssim 0.010$ ($A \lesssim 60$).
- $\Delta A/A \lesssim 0.012$ ($A \lesssim 80$).

In the framework of the presently ongoing PRESPEC-AGATA campaign at GSI, a comprehensive performance commissining experiment has been performed recently, complemented with extensive pulser calibration data. This data is presently being analysed. Results concerning LYCCA performance will be subject to a forthcoming paper, detailing analysis procedures as well as achieved detector, proton number, and mass number resolutions [27].

6. Summary and outlook towards HISPEC at FAIR-NUSTAR

The concept, design and prototype developments for the FAIR-NUSTAR detector system LYCCA have been described. LYCCA aims to discriminate relativistic heavy-ion reaction products at typical energies of 100-300 MeV/u. Valuable and timely feedback on the LYCCA design concept has been achieved during its early PRESPEC implementation of 12- and 16-module prototype versions of LYCCA at the GSI Helmholtzcentre for Heavy Ion Research in the years 2010-2014. With the basic LYCCA particle identification concept proven (cf. Sec. 5), further optimization on data analysis software algorithms is ongoing [27], and additional detectors and detector modules as well as electronics upgrades are foreseen towards the anticipated implementation of the complete LYCCA device for HISPEC experiments.

Concerning detectors, a very-large area plastic scintillator is being built to cover the approximate full 40-cm diameter of the downstream HISPEC beam pipe, i.e. the anticipated 26-module version of the LYCCA Wall. Concerning these telescopes of the LYCCA Wall, the aim is to be able to provide up to 30 CsI blocks each of the 'short' and 'long' version.

In terms of read-out and processing electronics, the LYCCA Wall telescopes are going to be upgraded to already existing and commissioned sampling electronics modules: for the CsI(Tl)-PD part, the preamplifier

signals are going to be digitized with some twenty 16-channel GSI-EE FEBEX3 cards [38] based on 14-bit 50 MHz sampling ADCs. The DSSSDs are going to be handled by custom made front-end electronics developed in the United Kingdom. It is based on a application specific integrated circuit design for the AIDA project [39]. Revised CFD-TDC concepts for the PMT signal processing of the large-area scintillators are to be investigated.

Finally, LYCCA is going to be readily available to support physics-driven Super-FRS commissioning towards FAIR-NUSTAR, either stand-alone or together with other FAIR-NUSTAR detectors and activities.

Acknowledgements

LYCCA has been enabled by financial contributions of The Swedish Research Council, the German BMBF, and the United Kingdom STFC. The Lund group acknowledges essential additional financial support from The Royal Physiographic Society in Lund and The Crafoord Foundation in Lund. The LYCCA collaboration is grateful for the help of in particular GSI staff during the first LYCCA commissioning phase.

References

[1] http://www.fair-center.eu/for-users/experiments/nustar.html
[2] http://www.fair-center.eu/en/for-users/experiments/nustar/experiments/hispecdespec.html
[3] http://www.fair-center.eu/en/for-users/experiments/nustar/experiments/super-frs.html
[4] S. Akkoyun *et al.*, Nuclear Instruments and Methods in Physics Research Section A 668 (2012).
[5] P. Boutachkov *et al.*, to be published.
[6] H. Geissel *et al.*, Nuclear Instruments and Methods in Physics Research Section B 70 (1992) 286.
[7] H.J. Wollersheim *et al.*, Nuclear Instruments and Methods in Physics Research Section A 573 (2005) 637.
[8] J. Eberth *et al.*, Nuclear Instruments and Methods in Physics Research Section A 369 (1996) 139.
[9] R. Lozeva *et al.*, Nuclear Instruments and Methods in Physics Research Section A 562 (2006) 298.
[10] M.J. Taylor *et al.*, Nuclear Instruments and Methods in Physics Research Section A 606 (2009) 589.
[11] D. Rudolph *et al.*, LYCCA Technical Design Report, FAIR-NUSTAR, June 2008, available at `http://www.nuclear.lu.se/english/research/basic_nuclear_physics/nustar/lycca/publications`.
[12] http://www.kns.com, Kulicke & Soffa, Manual *KS4523 Digital Bonder*.
[13] http://www.bluestarsilicones.com
[14] http://www.amcrys-h.com
[15] V. Avdeichikov *et al.*, Nuclear Instruments and Methods in Physics Research Section A 349 (1994) 216.
[16] V. Avdeichikov *et al.*, Nuclear Instruments and Methods in Physics Research Section A 439 (2000) 158.
[17] V. Avdeichikov *et al.*, Nuclear Instruments and Methods in Physics Research Section A 484 (2002) 251.
[18] D. Bédérède *et al.*, Nuclear Instruments and Methods in Physics Research Section A 518 (2004) 15.
[19] A.S. Barann, Bachelor thesis, Lund University, 2013, unpublished.
[20] J. Taprogge, Bachelor thesis, Universität zu Köln, 2009, unpublished.
[21] V. Avdeichikov *et al.*, Nuclear Instruments and Methods in Physics Research Section A 466 (2001) 427.
[22] V. Avdeichikov *et al.*, Nuclear Instruments and Methods in Physics Research Section A 501 (2003) 505.
[23] D.D. DiJulio *et al.*, Nuclear Instruments and Methods in Physics Research Section A 612 (2009) 127.
[24] R. Hoischen *et al.*, Nuclear Instruments and Methods in Physics Research Section A 654 (2011) 354.
[25] F. Schirru *et al.*, J. Instrum. **7**, P05005 (2012).
[26] R. Hoischen, PhD thesis, Lund University, LUNFD6 / (NFFR - 1032) / 1-138 / (2011), ISBN 978-91-7473-090-6.
[27] LYCCA Collaboration, to be published.
[28] P. Moritz *et al.*, Diamond and Related Materials **10**, 1765 (2001).
[29] M.Ciobanu *et al.*, IEEE Transactions on Nuclear Science **58** 4 (2011).
[30] J. Taprogge, Masters thesis, Universität zu Köln, 2011, unpublished.
[31] A. Wendt, PhD thesis, Universitt zu Köln, ISBN 978-3-8439-0860-3 (2013).
[32] Phillips Scientific, www.phillipsscientific.com/
[33] ISEG GmbH, www.iseg-hv.com/
[34] G. Pascovici *et al.*, WSEAS Trans. Circuits and Systems Vol. **7** (6), 470 (2008).
[35] B. Kuo and F. Golnaraghi, Automatic Control Systems, John Willey & Sons Inc., 2003.
[36] mesytec GmbH, www.mesytec.com/
[37] L. Scruton, PhD thesis, University of York, 2013.
[38] J. Hoffmann, N. Kurz, S. Loechner, S. Minami, W. Ott, I. Rusanov, S. Voltz and P. Wieczorek, GSI Scientific Report 2011, GSI Report 2012-1 (2012).
[39] D. Braga, P.J. Coleman-Smith, T. Davinson, I.H. Lazarus, R.D. Page, and S. Thomas, IEEE Nucl. Sci. Symp. Conf. Record N27-4 (2009); http://www.ph.ed.ac.uk/~td/AIDA/.